A universal velocity transformation for boundary layers with pressure gradients

Peng E S Chen[1] †, Wen Wu [2], Kevin P. Griffin [3,5], Yipeng Shi [1], and Xiang I A Yang [4]

[1]Department of Mechanics and Engineering Science, Peking University, Beijing, China, 100871

[2]Department of Mechanical Engineering, University of Mississippi, Mississippi, USA, 38677

[3]Center for Turbulence Research, Stanford University, Stanford, USA, 94305

[4]Mechanical Engineering, Pennsylvania State University, Pennsylvania, USA, 16802

[5]National Renewable Energy Laboratory, Colorado, USA, 80401

(Received xx; revised xx; accepted xx)

The logarithmic law of the wall does not capture the mean flow when a boundary layer is subjected to a strong pressure gradient. In such a boundary layer, the mean flow is affected by the spatio-temporal history of the imposed pressure gradient; and accounting for history effects remains a challenge. This work aims to develop a universal mean flow scaling for boundary layers subjected to arbitrary adverse or/and favorable pressure gradients. We derive from the Navier-Stokes equation a velocity transformation that accounts for the history effects and maps the mean flow to the canonical law of the wall. The transformation is tested against channel flows with a suddenly imposed adverse or favorable pressure gradient, boundary layer flows subjected to an adverse pressure gradient, and Couette-Poiseuille flows with a streamwise pressure gradient. It is found that the transformed velocity profiles closely follow the equilibrium law of the wall.

1. Introduction

Boundary layers subjected to favorable pressure gradients (FPGs) or adverse pressure gradients (APGs) are common in fluid engineering. In the past 30 years, many have studied boundary layers with pressure gradients , including theory work (Perry *et al.* 1998; Wei *et al.* 2007; Nickels 2004; Wei *et al.* 2017; Subrahmanyam *et al.* 2022), experimental work (Aubertine & Eaton 2005; Harun *et al.* 2013; Parthasarathy & Saxton-Fox 2022; Volino 2020; Romero *et al.* 2022*b*), and computational work (Lee & Sung 2009; Inoue *et al.* 2013; Lee 2017; Kitsios *et al.* 2017; Subrahmanyam *et al.* 2023), to name a few of the previous work. It was known that the mean flow responds to pressure gradients faster than the turbulence. It has also been found that there are history effects, and the law of the wall loses its predictive power. However, it is unclear how one can account for history effects in a mean flow scaling. Consequently, no good mean flow scaling exists for boundary layers with pressure gradients. This work aims to account for history effects in the mean flow scaling and establish a universal mean flow scaling for boundary layers subjected to arbitrary adverse and favorable pressure gradients.

We begin our discussion by estimating the pressure gradients encountered in engineering flows. Consider, e.g., the boundary layer on the suction side of an airfoil, such as sterns on an underwater vehicle or a turbine blade. At large angles of attack, the pressure gradient

† Email address for correspondence: chenpeng66@pku.edu.cn

causes an appreciable change in the fluid velocity. An order-of-the-magnitude estimate of the pressure gradient is

$$\frac{dP}{ds} = \alpha \frac{\rho U_0^2}{c}, \tag{1.1}$$

where dP/ds is the pressure gradient along a streamline, U_0 is the velocity of the incoming fluid, c is the chord length, and α is an order 0.1 factor. Define

$$\Pi \equiv \frac{\delta}{\rho \tau_w} \frac{dP}{ds}, \tag{1.2}$$

where δ is the boundary layer thickness, and $\tau_w = \nu dU/dy$ is the wall-shear stress. We have

$$\Pi = \frac{\delta}{\rho \tau_w} \frac{\alpha \rho U_0^2}{c} = \frac{2\alpha \delta/c}{C_f}. \tag{1.3}$$

A rough estimate according to (Anderson 2011) is

$$C_f \sim O(10^{-4} - 10^{-3}), \quad \alpha\delta/c \sim O(0.001 - 0.01), \tag{1.4}$$

which leads to

$$\Pi \sim O(1) \text{ to } O(100). \tag{1.5}$$

Following this estimate, we limit ourselves to $|\Pi|$ between 1 and 100. Flows subjected to a pressure gradient with $\Pi < 1$ will be in a quasi-equilibrium state and flows subjected to a pressure gradient with $\Pi > 100$ are rare.

Consider the scaling of the mean velocity. The canonical law of the wall (LoW) provides a good working approximation of the mean flow in a zero-pressure-gradient (ZPG) boundary layer. Here, the LoW refers to the scaling of the mean flow in the constant stress layer (or the inner layer), where the inner scaled velocity follows a linear and a logarithmic scaling of the inner scaled distance from the wall for $y \lesssim 5\nu/u_\tau$ and $\nu/u_\tau \ll y \ll \delta$, respectively:

$$\begin{aligned} U^+ &= y^+, \quad \text{for } y \lesssim 5\nu/u_\tau, \\ U^+ &= \frac{1}{\kappa} \log(y^+) + B, \quad \text{for } \nu/u_\tau \ll y \ll \delta, \end{aligned} \tag{1.6}$$

the behavior of the mean flow in the buffer layer is also a function of y^+ only but there is not an accepted explicit expression. Here $U^+ = U/u_\tau$, U is the mean velocity, u_τ is the friction velocity, $y^+ = yu_\tau/\nu$, ν is the kinematic viscosity, y is the wall-normal coordinate, δ is an outer length scale (e.g., boundary-layer thickness, half-channel height, pipe radius), $\kappa \approx 0.4$ is the von Kármán constant (keeping only one significant digit), and $B \approx 5$ is a constant (Kim *et al.* 1987; Marusic *et al.* 2013; Smits *et al.* 2011; Monty *et al.* 2009; Morrill-Winter *et al.* 2017). Equation (1.6) fails when the boundary layer is subjected to a strong pressure gradient (Spalart & Watmuff 1993; Nagib & Chauhan 2008; Monty *et al.* 2011). For illustrative purposes, consider the model problem sketched in figure 1 (a), where a fully developed channel is subjected to a suddenly imposed APG. Figure 1(b) shows the velocity profiles in inner units, at a few time instants after an APG $\Pi = 100$ is suddenly imposed on a $Re_{\tau,0} = u_{\tau,0}\delta/\nu = 1000$ channel. Beside that the velocity is above the log law, the region within which $U^+ = y^+$ also retreats, which is quite peculiar. We discuss the scaling of the mean flow in the viscous sublayer in Appendix A. Define

$$\Delta p^+ \equiv \frac{\nu}{\rho u_\tau^3} \frac{dP}{dx}, \text{ and } \beta \equiv \frac{\delta^*}{\rho u_\tau^2} \frac{dP}{dx}, \tag{1.7}$$

which are common non-dimensional measures of the APG with β being the Clauser pressure

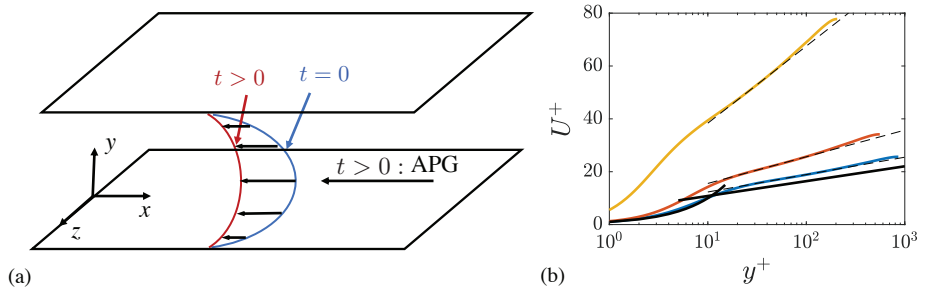

Figure 1: (a) Schematic of the model problem. A fully developed channel is subjected to a suddenly imposed APG and decelerates as a result. (b) Mean velocity profiles at a few time instants. The flow is initially at a Reynolds number $Re_\tau = 1000$. An APG $\Pi = +100$ is imposed at $t = 0$. Shown here are velocity profiles at $tu_{\tau,0}/\delta = 0.005$ (blue), 0.035 (red), and 0.065 (yellow). The profiles are normalized with the density ρ, the viscosity μ and the instantaneous wall shear stress $\tau_w(t)$. The dashed lines correspond to (1.6), but we allow κ and B in (1.6) to vary. Best fits yield $\kappa = 0.35, 0.23, 0.079$, $B = 5.8, 5.48, 9.2$ at $tu_{\tau,0}/\delta = 0.005, 0.035$, and 0.065, respectively.

gradient coefficient, δ^* being the displacement height, and ρ being the fluid density. The displacement height in a channel flow is defined as

$$\delta^* = \int_0^\delta \left(1 - \frac{U}{U_c}\right) dy, \tag{1.8}$$

where δ is the half channel height, and U_c is the mean streamwise velocity at the center line. Here, the Clauser parameter is the ratio of the two quantities which cause the momentum thickness to increase in a spatially developing boundary layer (in the momentum integral equation). We will report both Δp^+ (Knopp *et al.* 2021; Lozano-Durán *et al.* 2020; Johnstone *et al.* 2010; Nickels 2004) and β in the following for completeness. For this model problem, $\Delta p^+ = 0.1$, $\beta = 11.6$ at the initial state.

We see clear history effects in figure 1 (b): the same force leads to different velocity profiles at different time instances. This is quite expected: since $F = ma$ and $Ft = m\Delta V$, the change in the fluid velocity is not solely determined by the instantaneous force but by the force acting on the fluid parcel for a period of time. Such history effects were also noted in Perry *et al.* (2002), Bobke *et al.* (2017), Volino (2020), Romero *et al.* (2022*b*), among others. We see from figure 1 (b) that the law of the wall in (1.6) with $\kappa = 0.4$ and $B = 5$ do not fit the data, not even the lower part of the velocity profiles, which is in contrast to Galbraith *et al.* (1977); Perry (1966); Spalart & Watmuff (1993). By varying the two "constants" in the log law, (1.6) fits the mean flow in the inner layer (Lee & Sung 2009; Knopp *et al.* 2021; Nagib & Chauhan 2008), as indicated by the black dash lines in figure 1. Here, the inner layer is the layer where the outer length scale does not play a role. In most studies, this layer is considered as $y \lesssim 0.15\delta$. However, tuning κ and B to fit data reduces the modeling task into a fitting exercise. The same can be said about the half power law(Knopp *et al.* 2021; Stratford 1959; Perry & Schofield 1973) and other laws (Ding *et al.* 2019; Perry 1966; Perry *et al.* 1966; Subrahmanyam *et al.* 2022), where one must also adjust the "constants" to fit data. Although the LoW also contains constants, i.e., κ and B, that must be calibrated against data, the fact that one does not need to adjust these two constants as a function of the Reynolds number makes the LoW "universal".

This work aims to establish a universal mean velocity scaling for wall-bounded flows subjected to arbitrary streamwise pressure gradients. Here, universality is with respect to the pressure gradient and its history. Mean flow scalings are usually explicit algebraic relations

with the normalized velocity on the left-hand side and the dependent variables on the right-hand side (Volino 2020; Romero *et al.* 2022*a*). If we were to follow this path, we would be looking for a scaling for U as a function of the inner and outer length scales and the history of the pressure gradients, which is a daunting task. Instead, we will pursue the idea of velocity transformation. This idea has received much attention in the high-Mach-number-flow literature (Huang & Coleman 1994; Trettel & Larsson 2016; Griffin *et al.* 2021; Volpiani *et al.* 2020). The goal of these transformations is to find U_m and L_m

$$U^* = \int_0^U \frac{1}{U_m} dU, \quad y^* = \int_0^y \frac{1}{L_m} dy. \tag{1.9}$$

such that the transformed velocity U^* follows the LoW and is a function of y^* irrespective of the density variation in the flow (Van Driest 1951; Modesti *et al.* 2019; Modesti & Pirozzoli 2019). We have a similar goal, but instead of equilibrium boundary layers, we study non-equilibrium boundary layers subjected to streamwise pressure gradients. The objective is to find a transformation such that the transformed velocity U^* follows the LoW and is a function of y^* only, irrespective of the pressure gradient.

The rest of the paper is organized as follows. We derive the transformation in §2. Details of the validation DNS data are presented in §3, followed by test results in §4. Last, we conclude in §5.

2. Velocity transformation

In this section, we derive the velocity transformation from the Navier-Stokes equation and discuss its properties.

2.1. *Assumptions*

The derivation assumes the following. First, the flow is incompressible. Second, the mean flow is two-dimensional. This holds when the pressure gradients are in the streamwise direction. Third, the boundary layer is thin with respect to its rate of growth. That is, the velocity gradient in the wall-normal direction is much larger than that in the streamwise direction (which is only approximately true for boundary layers but is exactly true for channel flow). This assumption limits the discussion to attached flows, i.e., before incipient separation. Fourth, the flow is assumed to be initially in an equilibrium state. That is, the mean flow initially conforms to the law of the wall. Fifth, it is assumed that a universal velocity transformation exists. Define

$$f \equiv \frac{dU^*}{dy^*}(1 + \nu_t^+). \tag{2.1}$$

Here, $\nu_t^+ = \nu_t/\nu$, ν is the kinematic viscosity, $\nu_t = -\langle uv \rangle / (dU/dy)$ is the eddy viscosity, and $-\langle uv \rangle$ is the Reynolds shear stress. By universality, f is a function of y^* only in the inner layer. Like any assumption in any theory, (2.1) facilitates mathematical derivations, and its validity must be verified empirically.

Since the transformed velocity U^* is a function of the transformed wall-normal coordinate y^* only, it follows from this universality assumption that ν_t^+ is also a function of only y^* only in the inner layer. In addition, because $f = 1$ in the inner layer of ZPG boundary-layer flows (due to the constant stress layer), the universality assumption implies that $f \equiv 1$ in all flows—in the layer where the outer length scale does not play a role. Note that we do not need to assume a constant stress layer. The function f, in general, is a function of y/δ.

2.2. *Governing equation*

The Reynolds averaged streamwise momentum equation reads

$$\frac{\partial U}{\partial t} + U\frac{\partial U}{\partial x} + V\frac{\partial U}{\partial y} = -\frac{1}{\rho}\frac{\partial P}{\partial x} + \frac{\partial \tau_{xx}}{\partial x} + \frac{\partial \tau_{xy}}{\partial y}, \tag{2.2}$$

where

$$\tau_{xx} = 2\nu\frac{\partial U}{\partial x} - \langle u'u' \rangle\,, \quad \tau_{xy} = \nu\left(\frac{\partial U}{\partial y} + \frac{\partial V}{\partial x}\right) - \langle u'v' \rangle\,. \tag{2.3}$$

The equation assumes incompressibility and two-dimensional mean flow. Hence, the $\partial/\partial z$ terms are dropped. Here, the upper case letters denote mean quantities; the lower case letters denote instantaneous quantities, $'$ denotes fluctuations, x, y, and z are the streamwise, wall-normal, and spanwise directions, U, V, W or u, v, w are the velocity in the three Cartesian directions, τ is the stress, $\langle\cdot\rangle$ denotes ensemble averaging. Invoking the thin boundary layer assumption leads to

$$\frac{\partial V}{\partial x} \ll \frac{\partial U}{\partial y}, \quad \frac{\partial \tau_{xx}}{\partial x} \ll \frac{\partial \tau_{xy}}{\partial y}. \tag{2.4}$$

It follows from equations (2.2), (2.3), and (2.4) that

$$\frac{\partial U}{\partial t} + U\frac{\partial U}{\partial x} + V\frac{\partial U}{\partial y} = -\frac{1}{\rho}\frac{\partial P}{\partial x} + \frac{\partial \tau_{xy}}{\partial y}, \tag{2.5}$$

where

$$\tau_{xy} = \nu\frac{\partial U}{\partial y} - \langle u'v' \rangle\,. \tag{2.6}$$

We take the y derivative of both sides of (2.5)

$$\left(\frac{\partial}{\partial t} + U\frac{\partial}{\partial x} + V\frac{\partial}{\partial y}\right)\frac{\partial U}{\partial y} + \frac{\partial U}{\partial y}\frac{\partial U}{\partial x} + \frac{\partial V}{\partial y}\frac{\partial U}{\partial y} = -\frac{1}{\rho}\frac{\partial^2 P}{\partial x \partial y} + \frac{\partial^2 \tau_{xy}}{\partial y^2}. \tag{2.7}$$

We seek to simplify (2.7). First, incompressiblity requires

$$\frac{\partial U}{\partial x} + \frac{\partial V}{\partial y} = 0. \tag{2.8}$$

Second, the y momentum equation reads:

$$\frac{1}{\rho}\frac{\partial P}{\partial y} + \frac{\partial \ \ v^2}{\partial y} = 0. \tag{2.9}$$

By applying $\partial/\partial x$ on both sides of (2.9), we have

$$\frac{1}{\rho}\frac{\partial^2 P}{\partial x \partial y} = \frac{\partial^2 \ \ v^2}{\partial x \partial y} \ll \frac{\partial^2 \tau_{xy}}{\partial y^2}, \tag{2.10}$$

due to the thin boundary layer assumption. Substituting (2.8) and (2.10) into (2.7) leads to

$$\frac{D}{Dt}\frac{\partial U}{\partial y} = \frac{\partial^2 \tau_{xy}}{\partial y^2}. \tag{2.11}$$

Invoking the eddy viscosity ν_t, the shear stress term is

$$\tau_{xy} = \nu\frac{\partial U}{\partial y}\left(1 + \nu_t^+\right). \tag{2.12}$$

Here, ν_t is unspecified. Hence, invoking ν_t introduces no modeling error. Plugging Eq. (1.9) and (2.1) into Eq. (2.12), we have

$$\frac{\nu}{\tau_{xy}}\frac{U_m}{L_m}f = 1. \tag{2.13}$$

2.3. *Transformation*

Equation (1.9) and (2.13) lead to

$$U^* = \int_0^U \frac{\nu f}{\tau_{xy}}\frac{dy^*}{dy}dU. \tag{2.14}$$

Equation (2.14) is a velocity transformation, but it requires knowledge of y^*. In the following, we derive a transformation that maps y^+ to y^*.

Integrating (2.11) in time, we have

$$\frac{\partial U}{\partial y} = \left(\frac{\partial U}{\partial y}\right)_0 + \int_0^t \frac{\partial^2 \tau_{xy}}{\partial y^2}Dt, \tag{2.15}$$

where the subscript 0 denotes quantities evaluated at the initial state. Note that the integration is lagrangian. Invoking the assumed initial state, the mean flow abides by the LoW, and therefore,

$$\left(\frac{\partial U}{\partial y}\right)_0 = \left(\frac{u_\tau^2}{\nu}\frac{1}{F(y^+)}\right)_0 = \frac{u_{\tau,0}^2}{\nu}\frac{1}{F(y_0^+)}, \tag{2.16}$$

where

$$F(y_0^+) = 1 + \kappa y_0^+\left(1 - \exp(-y_0^+/A)\right)^2, \tag{2.17}$$

is a damping function (Van Driest 1956; Kawai & Larsson 2012; Yang & Lv 2018), $A = 17$ is a constant, $y_0^+ = yu_{\tau,0}/\nu$, and $u_{\tau,0}$ is the friction velocity at the initial state. The use of the van Driest damping function is to give the equilibrium $\partial U/\partial y$ a closed expression. The derivation itself does not necessarily need such an approximation. An alternative definition for F is

$$F(y_0^+) = \frac{u_{\tau,0}^2}{\nu}\frac{1}{(\partial U/\partial y)_0}, \tag{2.18}$$

where we have left $(\partial U/\partial y)_0$ as is. Invoking (2.13) and the assumption that U^* follows the LoW, the left hand side of (2.15) is

$$\frac{\partial U}{\partial y} = \frac{\tau_{xy}}{\nu f}\frac{1}{F(y^*)}. \tag{2.19}$$

Substituting (2.19) into (2.15) and rearranging, we have

$$F(y^*) = \frac{1}{\left(\frac{\partial U}{\partial y}\right)_0 + \int_0^t \frac{\partial^2 \tau_{xy}}{\partial y^2}Dt}\frac{\tau_{xy}}{\nu f}. \tag{2.20}$$

Here, F is given in (2.17), $f \equiv 1$ for $y \ll \delta$, its value in the outer layer can be measured at the initial state (as a function of y/δ), and the derivative $(\partial U/\partial y)_0$ is known from the equilibrium LoW. Equations (2.20) and (2.14) are the transformations we are looking for.

2.4. *Further simplification*

We re-arrange (2.20) and (2.14) to put them into the standard as defined in (1.9). First, we

define

$$g \equiv \frac{\partial U/\partial y - (\partial U/\partial y)_0}{(\partial U/\partial y)_0}. \tag{2.21}$$

It follows from (2.15), (2.16), and (2.21) that

$$g = \frac{\nu F(y_0^+)}{u_{\tau,0}^2} \int_0^t \frac{\partial^2 \tau_{xy}}{\partial y^2} Dt. \tag{2.22}$$

Equation (2.22) and (2.20) together give

$$y^* = F^{-1}\left[\frac{1+g_w}{1+g}\frac{\tau^+}{f}F(y_0^+)\right]. \tag{2.23}$$

Here, F^{-1} denotes the inverse function of F, $\tau^+ = \tau_{xy}/\tau_{xy,w}$, and g_w is g evaluated at the wall. Notice that τ^+ is ill-defined at separation, and therefore our scaling is valid up to incipient separation. The term $(1+g_w)/(1+g)$ in (2.23) accounts for the history effects. Equation (2.23) gives

$$y^* = \int_0^y \frac{F(y^*)}{F'(y^*)}\left[\frac{f}{\tau^+}\frac{\partial}{\partial y}\left(\frac{\tau^+}{f}\right) - \frac{1}{1+g}\frac{\partial g}{\partial y} + \frac{F'(y_0^+)}{F(y_0^+)}\frac{dy_0^+}{dy}\right] dy. \tag{2.24}$$

Equations (2.24) and (2.14) give

$$U^* = \int_0^U \frac{\nu f}{\tau_{xy}}\frac{F(y^*)}{F'(y^*)}\left[\frac{f}{\tau^+}\frac{\partial}{\partial y}\left(\frac{\tau^+}{f}\right) - \frac{1}{1+g}\frac{\partial g}{\partial y} + \frac{F'(y_0^+)}{F(y_0^+)}\frac{dy_0^+}{dy}\right] dU. \tag{2.25}$$

Equations (2.24) and (2.25) are the velocity transformation.

2.5. *Discussion*

The transformations are collected below

$$\begin{aligned} y^* &= \int_0^y \frac{F(y^*)}{F'(y^*)}\left[\frac{f}{\tau^+}\frac{\partial}{\partial y}\left(\frac{\tau^+}{f}\right) - \frac{1}{1+g}\frac{\partial g}{\partial y} + \frac{F'(y_0^+)}{F(y_0^+)}\frac{dy_0^+}{dy}\right] dy, \\ U^* &= \int_0^U \frac{\nu f}{\tau_{xy}}\frac{F(y^*)}{F'(y^*)}\left[\frac{f}{\tau^+}\frac{\partial}{\partial y}\left(\frac{\tau^+}{f}\right) - \frac{1}{1+g}\frac{\partial g}{\partial y} + \frac{F'(y_0^+)}{F(y_0^+)}\frac{dy_0^+}{dy}\right] dU. \end{aligned} \tag{2.26}$$

We have the following remarks. Firstly, the transformation accounts for history effects through the time integral g. It is interesting to note that the integral is not weighted and therefore the flow does not "forget". In other words, an event at $t = 0$ and an event at a later time instant contribute equally to the transformation. Secondly, the transformation is valid in the outer layer as well. The function f is 1 in the inner layer and varies as a function of y/δ outside. By measuring f from the initial condition as a function of y/δ, the transformation should collapse all velocity profiles. Hence, the transformation avoids the constant stress layer assumption, at least formally. Thirdly, the transformation is presented as a descriptive tool for now. The transformation shows how history should be accounted for in mean flow scalings. It shows that pressure gradients do not affect the mean flow directly. Instead, they affect the shear stress, τ_{xy}, which then affects the mean flow. Closures for τ_{xy} and ν_t^+ are needed for the transformation, a topic we do not discuss here. Fourthly, the transformation involves a function inverse and therefore is not explicit.

In the following, we simplify and re-write the transformation for the log layer in a ZPG boundary layer, for Couette-Poiseuille flow, for a channel with a suddenly imposed streamwise pressure gradient, and for spatially developing boundary layers with streamwise pressure

gradients. First, for the log and the viscous layers, we have

$$\tau_{xy} = \text{Const.} \tag{2.27}$$

It follows that $g = 0$ and $\tau^+/f = 1$. Hence, for flows in the constant stress layer, the velocity transformation reduces to $U^* = U^+$ and $y^* = y^+$. Second, we consider the Couette-Poiseuille flow. Figure 2 (a) shows a schematic of the flow. The flow is subjected to an APG near one wall and an FPG near the other. The stress τ_{xy} is a linear function of y. The function f can be measured from the Couette flow, and $f = 1$. It follows that $g = 0$ and therefore, (2.23) becomes

$$F(y^*) = \tau^+ F(y^+). \tag{2.28}$$

The velocity transformation becomes

$$U^* = \int_0^U \frac{\nu f}{\tau_{xy}} \frac{F(y^*)}{F'(y^*)} \left(\frac{1}{\tau^+} \frac{\partial \tau^+}{\partial y} + \frac{F'(y^+)}{F(y^+)} \frac{dy^+}{dy} \right) dU. \tag{2.29}$$

Third, for channel flow with a suddenly imposed streamwise pressure gradient, the mean advection is 0, and therefore the Lagrangian integration degenerates to an Eulerian one, i.e., $Dt = dt$. It follows that (2.22) becomes

$$g = \frac{\nu F(y_0^+)}{u_{\tau,0}^2} \int_0^t \frac{\partial^2 \tau_{xy}}{\partial y^2} dt, \ y > 0. \tag{2.30}$$

Furthermore, measuring f from the initial condition, we have $f = 1 - y/\delta$. Fourth, for a spatially developing turbulent boundary layer with streamwise pressure gradients, Lagrangian integration is along the streamline, and (2.22) becomes

$$g = \frac{\nu F(y_0^+)}{u_{\tau,0}^2} \int_0^t \frac{\partial^2 \tau_{xy}}{\partial y^2} \frac{ds}{|\mathbf{U}|}, \ y > 0, \tag{2.31}$$

where ds is along a streamline, and $|\mathbf{U}|$ is the velocity magnitude. Equation (2.31) is singular at the wall because of the no-slip condition. However, this singularity is removable. We know that the velocity follows $U^+ = y^+$ sufficiently close to the wall irrespective of any non-equilibrium effects. Since U^* is a universal function of y^*, we must have $U^* = y^*$ sufficiently close to the wall as well. This directly gives $y^* = y^+$ at the wall, thereby removing the singularity at the wall.

3. Computational setup

To test the velocity transformation, we conduct DNSs of channel flows subjected to a suddenly imposed adverse or favorable pressure gradient. The flow is sketched in figure 1(a). It is a fully developed 2D turbulent channel. At $t = 0$, a constant pressure gradient dP/dx is suddenly imposed, subsequently held constant for the duration of the simulation. The mean flow evolves with time as a result.

Table 1 shows the DNS details. The nomenclature is as follows: R[$Re_{\tau,0}$/100]F/A[|Π|], where F is for FPG, and A is for APG. For APGs, Π is 1, 10, or 100, corresponding to a weak APG, a moderate APG, and a strong APG. For FPGs, $\Pi = -10$ or -100, corresponds to a moderate or a strong FPG. FPGs are not very challenging (or interesting) because the canonical LoW works reasonably well for flows with FPGs (Townsend 1956; Mellor & Gibson 1966), although FPGs have interesting effects on the eddies in the flow (Volino 2020). The initial Reynolds number is $Re_{\tau,0} = 544$ or 1000. The Reynolds number increases when an FPG is applied and decreases when an APG is applied. The size of the channel is

Case	$Re_{\tau,0}$	Π_0	β	$\Delta p^+ \times 10^3$	$L_x \times L_y \times L_z$	$n_x \times n_y \times n_z$	$\Delta x^+ \times \Delta y^+ \times \Delta_z^+$	N
R5A1	544	1	[0.13,3.88]	[1.84, 187]	$4\pi \times 2 \times 2\pi$	$576 \times 243 \times 540$	$11.8 \times (0.048, 7.23) \times 6.32$	3
R5A10	544	10	[1.31,20.1]	[18.4, 488]	$4\pi \times 2 \times 2\pi$	$576 \times 243 \times 540$	$11.8 \times (0.048, 7.23) \times 6.32$	4
R5A100	544	100	[19.9,49.5]	[184, 1245]	$4\pi \times 2 \times 2\pi$	$576 \times 243 \times 540$	$11.8 \times (0.048, 7.23) \times 6.32$	12
R5F10	544	-10	[-2.49,-0.94]	[-11.9, -7.6]	$4\pi \times 2 \times 2\pi$	$1024 \times 512 \times 1024$	$13.4 \times (0.13, 6.72) \times 6.70$	1
R5F100	544	-100	[-24.9,-1.93]	[-119, -16.1]	$4\pi \times 2 \times 2\pi$	$1024 \times 512 \times 1024$	$12.6 \times (0.12, 6.32) \times 6.29$	1
R10A10	1000	10	[1.17,8.17]	[10.1, 91.9]	$8\pi \times 2 \times 3\pi$	$2048 \times 512 \times 1536$	$12.3 \times (0.12, 6.15) \times 6.13$	2
R10A100	1000	100	[11.6,44.1]	[100, 573]	$8\pi \times 2 \times 3\pi$	$2048 \times 512 \times 1536$	$12.3 \times (0.12, 6.15) \times 6.13$	3

Table 1: DNS details of channel flows subjected to a suddenly imposed adverse ($\Pi > 0$) or favorable ($\Pi < 0$) pressure gradient. $Re_{\tau,0}$ is the initial Reynolds number. Π is positive for APG and negative for FPG. L_x, L_y, and L_z are the domain size in the streamwise, wall-normal, and spanwise directions. Here, normalization is by the half-channel height. n_x, n_y, and n_z are the number of grid points in the three Cartesian directions. Δx^+, Δy^+, and Δz^+ are the grid spacings in the three directions. For Δy^+, we list the resolution at the wall and the channel center. Here, we list the grid resolution at the beginning or the end of the DNSs. For $\Pi > 0$, a finer grid must be employed at the beginning than at the end, and we list the grid resolution at the beginning of the DNS and vice versa. N is the number of ensembles used to compute the flow statistics.

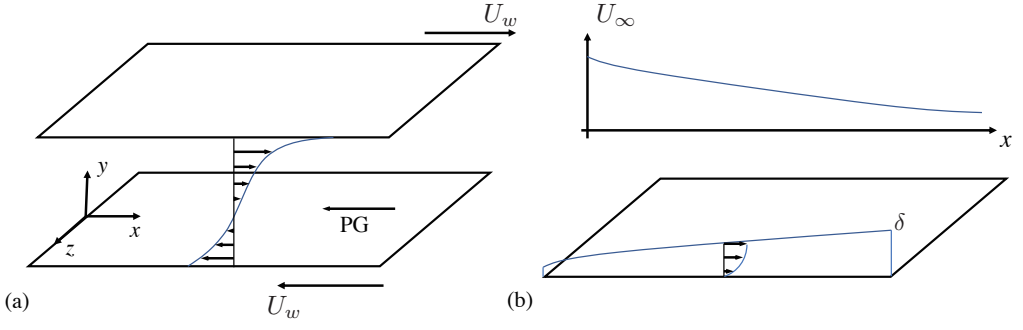

Figure 2: (a) A sketch of Couette-Poiseuille flow. The flow is subjected to an FPG near the top plate and an APG near the bottom plate (Coleman & Spalart (2015); Johnstone *et al.* (2010)); (b) A sketch of a boundary layer subjected to APGs. The pressure gradient is imposed by varying the freestream velocity. The reader is directed to Bobke *et al.* (2017) for more details.

$(4\pi \times 2 \times 2\pi)\delta$ for the R5 ($Re_{\tau,0} = 544$) cases and $(8\pi \times 2 \times 3\pi)\delta$ for the R10 ($Re_{\tau,0} = 1000$) cases. The domain sizes for the R5 and R10 cases are different because the initial fields were generated by different authors. Nonetheless, both domains are larger than that of the minimal channel (Lozano-Durán & Jiménez 2014). The grid resolution is comparable to that in Mathur *et al.* (2018) and Yang *et al.* (2021) and is such that the flow is well-resolved from the beginning to the end. We employ statistically un-correlated initial flow fields and repeat the simulations multiple times to get converged statistics following Lozano-Durán *et al.* (2020), Chung (2005), and He & Seddighi (2015). The code we use is the same as the one in Lee & Moser (2015). Details of the code can be found in Graham *et al.* (2016) and Lee & Moser (2015) and are not detailed here for brevity.

We will also use the boundary-layer data in Bobke *et al.* (2017), and the Couette-Poiseuille data in Coleman & Spalart (2015) and Johnstone *et al.* (2010). The flows are sketched in figure 2. Flow parameters that are relevant to this analysis are tabulated in Table 2. Further details are not shown here for brevity.

Case	Flow type	Ref.	Re_τ	Π	β	$\Delta p^+ \times 10^3$
CGSR5A	CP	Coleman *et al.* (2015)	589	+1.59	-	2.7
CGSR12F	CP	Coleman *et al.* (2015)	1210	-0.39	-	-0.32
JCSR3A	CP	Johnstone *et al.* (2010)	336	+1.24	-	3.7
JCSR6F	CP	Johnstone *et al.* (2010)	627	-0.36	-	-0.57
m13	APG-BL	Bobke *et al.* (2017)	[190; 896]	[3.80; 5.51]	[0.86, 1.49]	[5.0, 21.3]
m16	APG-BL	Bobke *et al.* (2017)	[189; 934]	[5.82; 8.67]	[1.55,2.55]	[10.9, 27.7]
m18	APG-BL	Bobke *et al.* (2017)	[192; 973]	[7.29; 12.5]	[2.15,4.07]	[16.0, 33.6]
b1	APG-BL	Bobke *et al.* (2017)	[190; 862]	≈ 4.11	≈ 1	[5.1, 14.3]
b2	APG-BL	Bobke *et al.* (2017)	[189; 910]	≈ 7.55	≈ 2	[10.6, 20.8]
ZPG	ZPG-BL	Schlatter & Örlü (2010)	[252; 1271]	0	0	0

Table 2: Details of the Couette-Poiseuille flows and the boundary-layer flows. CP is short for Couette Poiseuille. The nomenclature is [Initial of authors][Re_τ/100][PG]. Re_τ is the friction Reynolds number. Further details of the flows can be found in Coleman *et al.* (2015) and Johnstone *et al.* (2010) and are not repeated here for brevity. The velocity in a Couette-Poiseuille flow increases monotonically from one wall to the other. It is therefore not straightforward to define the heights of the boundary layers near the two walls. Consequently, defining β is not straightforward for Couette-Poiseulle flow. Here, BL is short for boundary layer. The nomenclature of the BL cases is the same as in Bobke *et al.* (2017). The range of Re_τ and Π are shown in the table. Note that for b1 and b2 cases, Π is approximately a constant, while for m13, m16 and m18 cases, it is varying. We also include the ZPG-BL data in Schlatter & Örlü (2010) for comparison purposes.

4. Results

4.1. *Channel flow results*

First, we present the channel flow results. Figures 3 and 4 show the mean velocity profiles in the APG cases. Figure 3 shows the R5 results, and figure 4 shows the R10 results. The results at other time instants are similar and are not shown here for brevity. In R5A1, a weak APG is applied, and the flow is at a quasi-equilibrium state. As a result, both U^+ and U^* follow the LoW. In R5A10 and R10A10, a moderate APG is applied, and we see noticeable deviations in U^+ from the LoW after the adverse pressure gradient has acted on the flow for some time at $t = O(10)$. On the other hand, the transformed velocity U^* follows the LoW closely at all time instants. In R5A100 and R10A100, a strong APG is applied. The viscous units fail to collapse the velocity profiles, and only U^* follows the LoW.

Figure 5 shows the mean velocity profiles in the two FPG cases. FPGs give rise to noticeable deviations from the LoW in R5F100 when the velocity and the wall-normal coordinate are normalized using the viscous units. Nonetheless, the transformed velocity profiles collapse and follow the LoW.

Per the universality assumption, the viscous scaled eddy viscosity is a universal function of the transformed wall-normal coordinate y^*. In section 2, we noted "like any assumption in any theory, (2.1) facilitates mathematical derivations, and its validity must be verified empirically." In the following, we test (2.1) against empirical data. Figures 6 and 7 show the eddy viscosity in the APG cases. Figure 6 shows the R5 results, and figure 7 shows the R10 results. The flow in R5A1 is at a quasi-equilibrium state, y^+ and y^* are not very different, and ν_t^+ collapse well when plotted as a function of both y^+ and y^*. In R5A10, R5A100, R10A10, and R10A100, the pressure gradients are strong, and the conventional viscous scaling does not collapse data and only the transformed wall-normal coordinate collapse data. Figure 8 shows the normalized eddy viscosity of the FPG cases. The results are similar to the APG

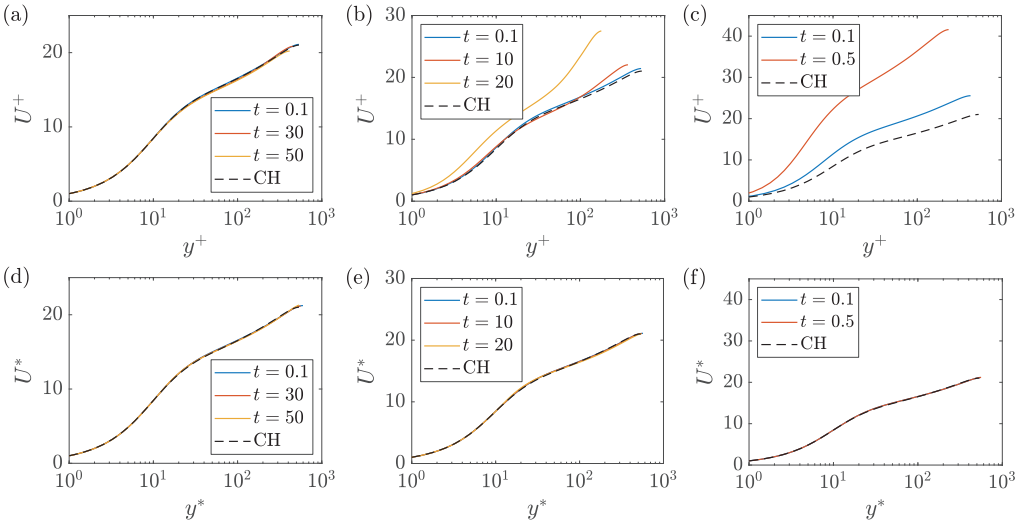

Figure 3: Mean velocity profiles at a few time instants. (a, b, c) U^+ as a function of y^+. Here, normalization is by the wall-shear stress at time t. (d, e, f) U^* as a function of y^*. Here, $U^*(y^*)$ is the transformed velocity. (a, d) R5A1. (b, e) R5A10. (c, f) R5A100. Here, time t is normalized with $\delta/u_{\tau,0}$. CH is the velocity profile in a fully developed $Re_\tau = 544$ channel.

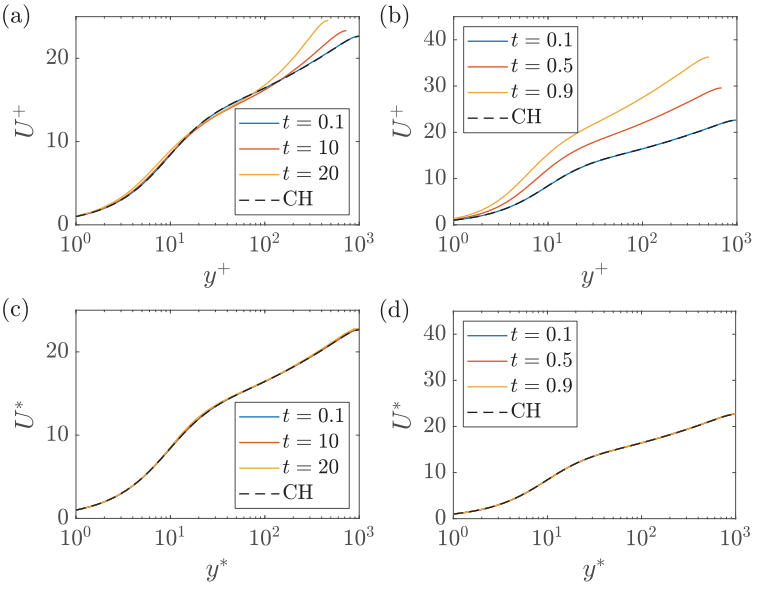

Figure 4: Mean velocity profiles at a few time instants. (a, b) U^+ as a function of y^+. Here, normalization is by the wall-shear stress at time t. (c, d) U^* as a function of y^*. Here, $U^*(y^*)$ is the transformed velocity. (a, c) R10A10. (b, d) R10A100. CH is the velocity profile in a fully developed $Re_\tau = 1000$ channel.

cases: the viscous scaling does not collapse data, whereas the transformed coordinate does. These results verify the universality assumption.

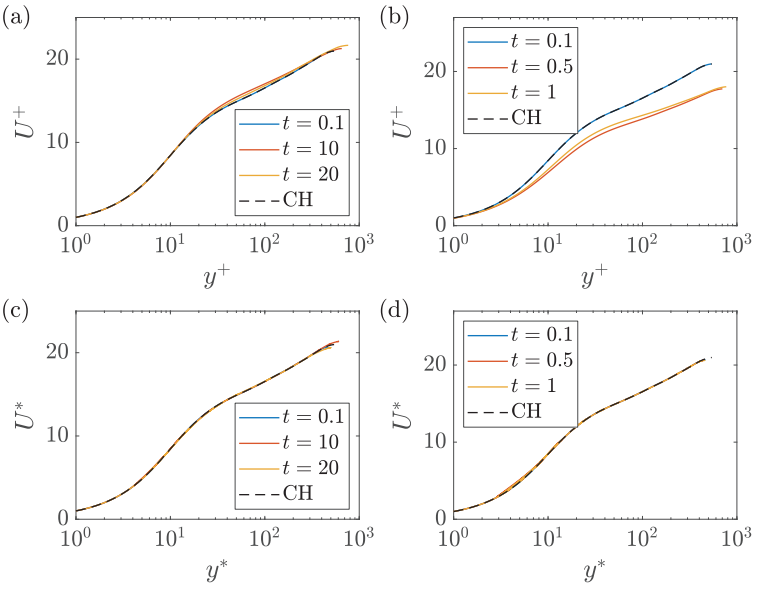

Figure 5: Mean velocity profiles at a few time instants. (a, b) U^+ as a function of y^+. Here, normalization is by the wall-shear stress at time t. (c, d) U^* as a function of y^*. Here, $U^*(y^*)$ is the transformed velocity. (a, c) R5F10. (b, d) R5F100. CH is the velocity profile in a fully developed $Re_\tau = 544$ channel.

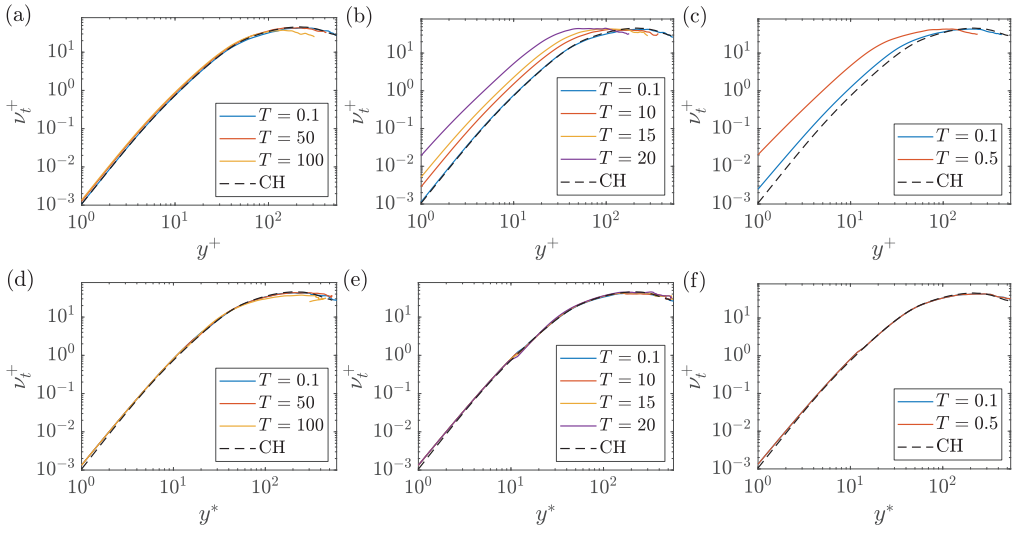

Figure 6: Eddy viscosity at various time instants. (a, b, c) ν_t^+ as a function of y^+. (d, e, f) ν_t^+ as a function of y^*. (a, d) R5A1. (b, e) R5A10. (c, f) R5A100.

4.2. *Couette Poiseuille and boundary-layer flows*

Next, we show the Couette-Poiseuille flow results. Figure 9 shows the mean velocity profiles before and after the transformation. The flows are subjected to fairly weak pressure gradients. As a result, the viscous scaled velocity profiles do not deviate far from the LoW, and the velocity transformation leads to a slightly better collapse of the velocity profiles.

Last, figure 10 shows the boundary layer results. The transformation collapses all profiles,

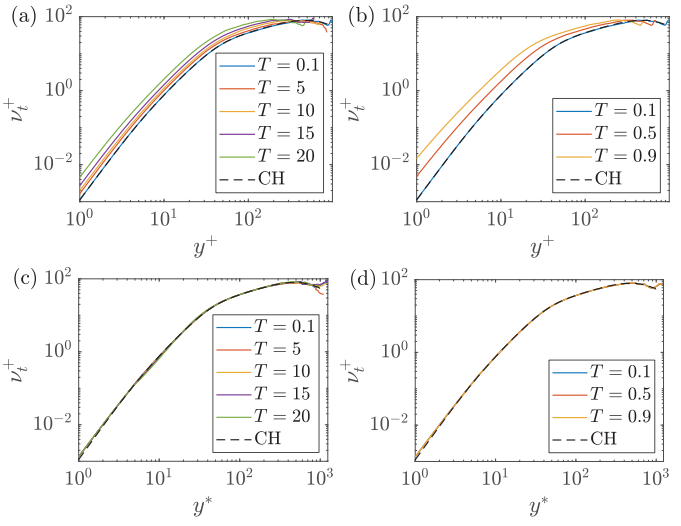

Figure 7: Same as figure 6 but for the R10 cases. (a, c) R10A10. (b, d) R10A100.

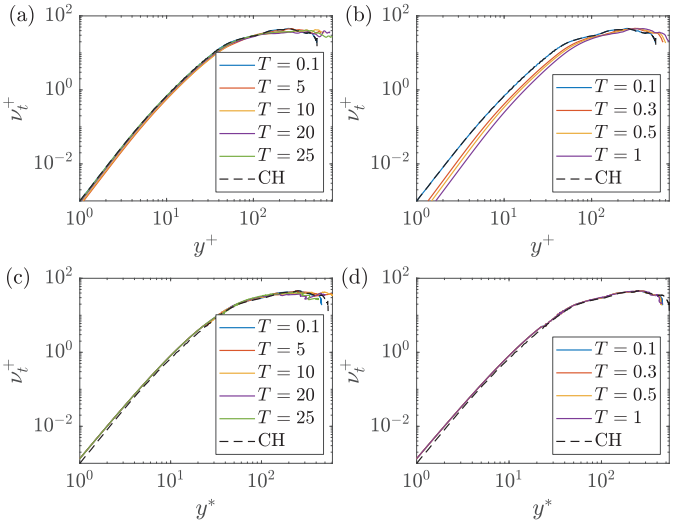

Figure 8: Same as figure 6 but for the R5F cases. (a, c) R5F10. (b, d) R5F100.

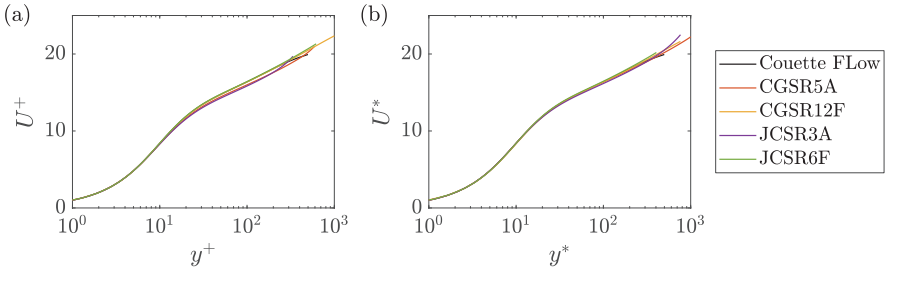

Figure 9: Mean velocity profiles in Couette-Poiseuille flows (a) before and (b) after the transformation.

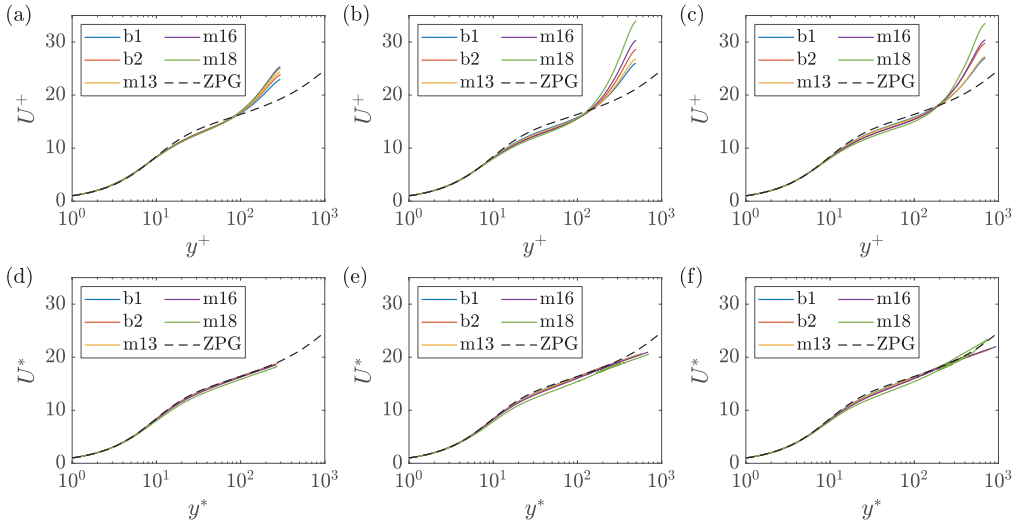

Figure 10: Mean velocity profiles in boundary-layer flows at multiple streamwise locations: (a, d) $Re_\tau = 300$; (b, e) $Re_\tau = 500$; (c, f) $Re_\tau = 700$. "ZPG" is the velocity profile in a zero-pressure-gradient boundary layer at $Re_\tau = 1272$.

and the transformed velocity profiles follow the LoW. However, the collapse is less convincing compared to the results in figures 3 to 4. We think this is a lack of statistical convergence—compared to channel flow, where one can average among many ensembles and in the two homogeneous directions, the boundary-layer is amenable to averaging in time and the spanwise direction. A lack of statistical convergence incurs errors in the derivative calculations, which in turn affect the quality of the data collapse– an aspect that needs further attention.

5. Conclusions

We derived a velocity transformation that maps the mean velocity profiles in boundary layers with pressure gradients to the canonical law of the wall before incipient separation. The NS equation alone does not give the transformation. Like the semi-local transformation that relies on the assumption that ν_t^+ is a universal function of y_{sl}^*, our transformation relies on (2.1), a direct consequence of which is that ν_t^+ is a universal function of y^*. In addition to (2.1), we assume two-dimensional attached mean flows at low speeds and the knowledge of the mean flow at the equilibrium condition.

The derived transformation contains mean flow information and shear-stress information only. History effects are accounted for via a Lagrangian integral of the total shear stress originating from the initial equilibrium state. The transformation suggests that it is the total shear stress that plays into the hysteresis in the mean flow. Furthermore, since the integration weights all historical events equally, the flow does not forget unless the effects of one event are canceled by another.

The validity of the transformation is tested in channel flows subjected to suddenly imposed pressure gradients, Couette-Poiseuille flows, and spatially-developing turbulent boundary layers with moderate adverse pressure gradients. We show that while the inner-unit scaled velocity profiles deviate from the LoW, the transformed profiles follow the LoW closely, irrespective of the streamwise pressure gradients. Further validation of the scaling will be pursued in future studies.

Last, we comment on the practicality of the present transformation. The LoW is the cornerstone of many wall-bounded turbulence models. However, since the LoW is valid for equilibrium boundary layers only, the reliance on the LoW is a major source of uncertainty in turbulence modeling. As a result, there has always been a need for universal mean flow scalings for non-equilibrium boundary layers. This work will help address that need. While this paper presented the velocity transformation as a descriptive tool, future work will explore its potential for predictive modeling. Consider, e.g., RANS modeling. At a given iteration, one would have a velocity field, which allows one to compute the eddy viscosity and the total shear stress to get to the next iteration. When computing the eddy viscosity in the wall layer, one often needs a damping function. The available damping functions are functions of y^+ (or constructed assuming it is a function of y^+), which is based on the law of the wall and therefore is not always accurate. Our scaling can be used to augment the damping function. The resulting damping function would depend on the Lagrangian history of the total shear stress, but the information is solved for and is available in the simulation. We will leave such practical applications to future studies.

Acknowledgments

Chen and Shi acknowledge financial support from NSFC 91752202. Yang acknowledges the 2022 CTR summer program and Office of Naval Research, contract number N000142012315 for financial support. Wu acknowledges support from NSF grant No. 2131942 for visiting CTR in the summer of 2022. Yang thanks Parviz Moin, Ahmed Elnahhas, Rahul Agrawal, Adrian Lozano-Duran, Jane Bae, Olaf Marxen, Michael Cui, and Mostafa Momen for their generous help during his stay at Stanford. Yang thanks the comments from Johan Larsson, George Huang, Sergio Pirozzoli, and Ivan Marusic. Griffin is supported by the Exascale Computing Project (grant 17-SC-20-SC), a collaborative effort of two US Department of Energy organizations (Office of Science and the National Nuclear Security Administration) responsible for the planning and preparation of a capable exascale ecosystem, including software, applications, hardware, advanced system engineering, and early testbed platforms, in support of the nation's exascale computing imperative. This work was authored in part by the National Renewable Energy Laboratory, operated by Alliance for Sustainable Energy, LLC, for the U.S. Department of Energy (DOE) under Contract No. DE-AC36-08GO28308. The views expressed in the article do not necessarily represent the views of the DOE or the U.S. Government. The U.S. Government retains and the publisher, by accepting the article for publication, acknowledges that the U.S. Government retains a nonexclusive, paid-up, irrevocable, worldwide license to publish or reproduce the published form of this work, or allow others to do so, for U.S. Government purposes.

Declaration of Interests

The authors report no conflict of interest.

Appendix A. Mean flow scaling in the viscous sublayer

We discuss the scaling of the mean flow in the viscous sublayer. First, expanding the mean velocity according to Taylor series in the wall layer gives

$$U = \left.\frac{\partial U}{\partial y}\right|_w y + \frac{1}{2}\left.\frac{\partial^2 U}{\partial y^2}\right|_w y^2 + \mathcal{O}(y^3). \tag{A 1}$$

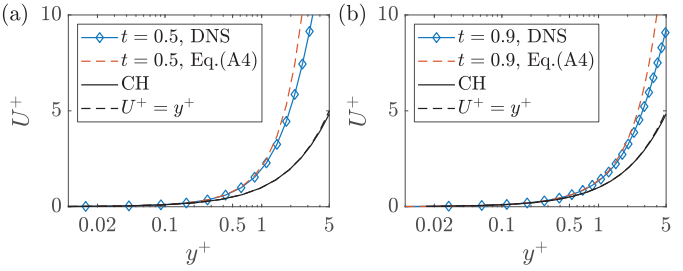

Figure 11: The mean velocity profile in the viscous sublayer of (a) R5A100 and (b) R10A100. The markers show the grid point locations.

The definition of τ_w gives

$$\left.\frac{\partial U}{\partial y}\right|_w = \frac{\tau_w(t)}{\nu}. \tag{A 2}$$

Evaluating the NS equation at the wall gives:

$$\left.\frac{\partial^2 U}{\partial y^2}\right|_w = \frac{P_x}{\rho\nu}. \tag{A 3}$$

Here, $P_x = dP/dx$. Second, substitute (A 2) and (A 3) into (A 1), we have

$$U^+ = y^+ + \frac{P_x\nu}{2\rho{\tau_w}^{3/2}}y^{+2} + \mathcal{O}(y^3), \tag{A 4}$$

where $U^+ = U/u_\tau(t)$, $y^+ = u_\tau(t)y/\nu$, $u_\tau(t) = \sqrt{\tau_w(t)/\rho}$, and ν is the kinematic viscosity. The second term is subjected to the effect of pressure gradients. This explains the deviation of the mean flow from the canonical linear scaling in the viscous sublayer.

For an equilibrium channel, $P_x\delta/(2\rho\tau_w Re_\tau) = -0.5/(Re_\tau)$, and the second term in the Taylor expansion is $-0.001y^{+2}$, which amounts to -0.025 at $y^+ = 5$. For a boundary layer subjected to a strong adverse pressure gradient, e.g., case R5A100, $P_x\delta/(2\rho\tau_w Re_\tau) = 50/Re_\tau \approx 0.1$, and the second term in the Taylor expansion is $0.1y^{+2}$, which amounts to 2.5 at $y^+ = 5$.

Figure 11 shows the mean velocity profiles in the viscous sublayer layer. The profiles are normalized via the wall stress, viscosity, and fluid density. For brevity, we present results in the two cases with the strongest adverse pressure gradients. The time instants are such that the effects of the imposed adverse pressure gradients have already manifested. We have the following two observations. Firstly, the mean velocity profiles follow the linear scaling up to about $y^+ \approx 0.4$ and 0.7 in (a) and (b), respectively, and this region contains 6 and 9 grid points in (a) and (b). Secondly, the quadratic scaling (A4) is a more powerful scaling than the linear scaling.

REFERENCES

Anderson, John 2011 *Fundamentals of Aerodynamics*. McGraw Hill.

Aubertine, Carolyn D & Eaton, John K 2005 Turbulence development in a non-equilibrium turbulent boundary layer with mild adverse pressure gradient. *J. Fluid Mech.* **532**, 345–364.

Bobke, Alexandra, Vinuesa, Ricardo, Örlü, Ramis & Schlatter, Philipp 2017 History effects and near equilibrium in adverse-pressure-gradient turbulent boundary layers. *J. Fluid Mech.* **820**, 667–692.

Chung, Yongmann M 2005 Unsteady turbulent flow with sudden pressure gradient changes. *International journal for numerical methods in fluids* **47** (8-9), 925–930.

425 Coleman, GN, Garbaruk, A & Spalart, PR 2015 Direct numerical simulation, theories and modelling of
426 wall turbulence with a range of pressure gradients. *Flow Turbul. Combust.* **95**, 261–276.
427 Coleman, Gary N & Spalart, Philippe R 2015 Direct numerical simulation of turbulent Couette-Poiseuille
428 flow with zero skin friction. In *European Turbulence Conference 2015 (ETC 15)*.
429 Ding, Liuyang, Saxton-Fox, Theresa, Hultmark, Marcus & Smits, AJ 2019 Effects of pressure
430 gradients and streamline curvature on the statistics of a turbulent pipe flow. In *11th International*
431 *Symposium on Turbulence and Shear Flow Phenomena, TSFP 2019*.
432 Galbraith, RA McD, Sjolander, S & Head, MR 1977 Mixing length in the wall region of turbulent
433 boundary layers. *Aeronaut Quart* **28**, 97–110.
434 Graham, J, Kanov, K, Yang, X I A, Lee, M, Malaya, N, Lalescu, CC, Burns, R, Eyink, G, Szalay,
435 A, Moser, RD & others 2016 A web services accessible database of turbulent channel flow and its
436 use for testing a new integral wall model for LES. *J. Turbul* **17**, 181–215.
437 Griffin, Kevin Patrick, Fu, Lin & Moin, Parviz 2021 Velocity transformation for compressible wall-
438 bounded turbulent flows with and without heat transfer. *PNAS* **118**, e2111144118.
439 Harun, Zambri, Monty, Jason P, Mathis, Romain & Marusic, Ivan 2013 Pressure gradient effects on
440 the large-scale structure of turbulent boundary layers. *J. Fluid Mech.* **715**, 477–498.
441 He, S & Seddighi, M 2015 Transition of transient channel flow after a change in Reynolds number. *J. Fluid*
442 *Mech.* **764**, 395–427.
443 Huang, PG & Coleman, Gary N 1994 Van Driest transformation and compressible wall-bounded flows.
444 *AIAA J* **32**, 2110–2113.
445 Inoue, M, Pullin, DI, Harun, Zambri & Marusic, I 2013 LES of the adverse-pressure gradient turbulent
446 boundary layer. *Int J Heat Fluid Flow* **44**, 293–300.
447 Johnstone, Roderick, Coleman, Gary N & Spalart, Philippe R 2010 The resilience of the logarithmic
448 law to pressure gradients: evidence from direct numerical simulation. *J. Fluid Mech.* **643**, 163–175.
449 Kawai, Soshi & Larsson, Johan 2012 Wall-modeling in large eddy simulation: Length scales, grid
450 resolution, and accuracy. *Phys. Fluids* **24**, 015105.
451 Kim, John, Moin, Parviz & Moser, Robert 1987 Turbulence statistics in fully developed channel flow at
452 low Reynolds number. *J. Fluid Mech.* **177**, 133–166.
453 Kitsios, Vassili, Sekimoto, Atsushi, Atkinson, Callum, Sillero, Juan A, Borrell, Guillem, Gungor,
454 Ayse G, Jiménez, Javier & Soria, Julio 2017 Direct numerical simulation of a self-similar adverse
455 pressure gradient turbulent boundary layer at the verge of separation. *J. Fluid Mech.* **829**, 392–419.
456 Knopp, Tobias, Reuther, Nico, Novara, Matteo, Schanz, Daniel, Schülein, Erich, Schröder,
457 Andreas & Kähler, CJ 2021 Experimental analysis of the log law at adverse pressure gradient. *J.*
458 *Fluid Mech.* **918**, A17.
459 Lee, Jae Hwa 2017 Large-scale motions in turbulent boundary layers subjected to adverse pressure gradients.
460 *J. Fluid Mech.* **810**, 323–361.
461 Lee, Joung-Ho & Sung, Hyung Jin 2009 Structures in turbulent boundary layers subjected to adverse
462 pressure gradients. *J. Fluid Mech.* **639**, 101–131.
463 Lee, Myoungkyu & Moser, Robert D 2015 Direct numerical simulation of turbulent channel flow up to
464 $\mathrm{Re}_\tau \approx 5200$. *J. Fluid Mech.* **774**, 395–415.
465 Lozano-Durán, Adrián, Giometto, Marco G, Park, George Ilhwan & Moin, Parviz 2020 Non-
466 equilibrium three-dimensional boundary layers at moderate Reynolds numbers. *J. Fluid Mech.* **883**,
467 A20.
468 Lozano-Durán, Adrián & Jiménez, Javier 2014 Effect of the computational domain on direct simulations
469 of turbulent channels up to $\mathrm{Re}_\tau = 4200$. *Phys. Fluids* **26**, 011702.
470 Marusic, Ivan, Monty, Jason P, Hultmark, Marcus & Smits, Alexander J 2013 On the logarithmic
471 region in wall turbulence. *J. Fluid Mech.* **716**, R3.
472 Mathur, A, Gorji, S, He, S, Seddighi, M, Vardy, AE, O'Donoghue, T & Pokrajac, D 2018 Temporal
473 acceleration of a turbulent channel flow. *J. Fluid Mech.* **835**, 471–490.
474 Mellor, GL & Gibson, DM 1966 Equilibrium turbulent boundary layers. *J. Fluid Mech.* **24**, 225–253.
475 Modesti, Davide & Pirozzoli, Sergio 2019 Direct numerical simulation of supersonic pipe flow at
476 moderate Reynolds number. *Int J Heat Fluid Flow* **76**, 100–112.
477 Modesti, Davide, Pirozzoli, Sergio & Grasso, Francesco 2019 Direct numerical simulation of
478 developed compressible flow in square ducts. *Int J Heat Fluid Flow* **76**, 130–140.
479 Monty, JP, Hutchins, N, Ng, HCH, Marusic, I & Chong, MS 2009 A comparison of turbulent pipe,
480 channel and boundary layer flows. *J. Fluid Mech.* **632**, 431–442.

Monty, Jason P, Harun, Zambri & Marusic, I 2011 A parametric study of adverse pressure gradient turbulent boundary layers. *Int J Heat Fluid Flow* **32**, 575–585.

Morrill-Winter, Caleb, Philip, Jimmy & Klewicki, Joseph 2017 An invariant representation of mean inertia: theoretical basis for a log law in turbulent boundary layers. *J. Fluid Mech.* **813**, 594–617.

Nagib, Hassan M & Chauhan, Kapil A 2008 Variations of von Kármán coefficient in canonical flows. *Phys. Fluids* **20** (10), 101518.

Nickels, TB 2004 Inner scaling for wall-bounded flows subject to large pressure gradients. *J. Fluid Mech.* **521**, 217–239.

Parthasarathy, Aadhy & Saxton-Fox, Theresa 2022 A novel experimental facility to impose unsteady pressure gradients on turbulent boundary layers. *Experiments in Fluids* **63** (6), 1–14.

Perry, AE 1966 Turbulent boundary layers in decreasing adverse pressure gradients. *J. Fluid Mech.* **26**, 481–506.

Perry, AE, Bell, JB & Joubert, PN 1966 Velocity and temperature profiles in adverse pressure gradient turbulent boundary layers. *J. Fluid Mech.* **25** (2), 299–320.

Perry, AE, Marusic, I & Jones, MB 1998 New evolution equations for turbulent boundary layers in arbitrary pressure gradients. *Sadhana* **23** (5), 443–457.

Perry, AE, Marusic, Ivan & Jones, MB 2002 On the streamwise evolution of turbulent boundary layers in arbitrary pressure gradients. *J. Fluid Mech.* **461**, 61–91.

Perry, AE & Schofield, WH 1973 Mean velocity and shear stress distributions in turbulent boundary layers. *The Physics of Fluids* **16** (12), 2068–2074.

Romero, SK, Zimmerman, SJ, Philip, J & Klewicki, JC 2022*a* Stress equation based scaling framework for adverse pressure gradient turbulent boundary layers. *Int J Heat Fluid Flow* **93**, 108885.

Romero, Sylvia, Zimmerman, Spencer, Philip, Jimmy, White, Christopher & Klewicki, Joseph 2022*b* Properties of the inertial sublayer in adverse pressure-gradient turbulent boundary layers. *J. Fluid Mech.* **937**, A30.

Schlatter, Philipp & Örlü, Ramis 2010 Assessment of direct numerical simulation data of turbulent boundary layers. *J. Fluid Mech.* **659**, 116–126.

Smits, Alexander J, McKeon, Beverley J & Marusic, Ivan 2011 High–Reynolds number wall turbulence. *Ann. Rev. Fluid Mech.* **43**, 353–375.

Spalart, Philippe R & Watmuff, Jonathan H 1993 Experimental and numerical study of a turbulent boundary layer with pressure gradients. *J. Fluid Mech.* **249**, 337–371.

Stratford, BS 1959 The prediction of separation of the turbulent boundary layer. *J. Fluid Mech.* **5** (1), 1–16.

Subrahmanyam, Matthew, Xu, Zan, Cantwell, Brian & Alonso, Juan J 2023 A new wall-stress model for large-eddy simulations. In *AIAA SCITECH 2023 Forum*, p. 0285.

Subrahmanyam, Matthew A, Cantwell, Brian J & Alonso, Juan J 2022 A universal velocity profile for turbulent wall flows including adverse pressure gradient boundary layers. *J. Fluid Mech.* **933**, A16.

Townsend, AA 1956 The properties of equilibrium boundary layers. *J. Fluid Mech.* **1**, 561–573.

Trettel, Andrew & Larsson, Johan 2016 Mean velocity scaling for compressible wall turbulence with heat transfer. *Phys. Fluids* **28**, 026102.

Van Driest, Edward R 1951 Turbulent boundary layer in compressible fluids. *Journal of the Aeronautical Sciences* **18** (3), 145–160.

Van Driest, Edward R 1956 On turbulent flow near a wall. *Journal of the Aeronautical Sciences* **23** (11), 1007–1011.

Volino, Ralph J 2020 Non-equilibrium development in turbulent boundary layers with changing pressure gradients. *J. Fluid Mech.* **897**, A2.

Volpiani, Pedro S, Iyer, Prahladh S, Pirozzoli, Sergio & Larsson, Johan 2020 Data-driven compressibility transformation for turbulent wall layers. *Phys. Rev. Fluids* **5** (5), 052602.

Wei, Tie, Fife, Paul & Klewicki, Joseph 2007 On scaling the mean momentum balance and its solutions in turbulent Couette–Poiseuille flow. *J. Fluid Mech.* **573**, 371–398.

Wei, Tie, Maciel, Yvan & Klewicki, Joseph 2017 Integral analysis of boundary layer flows with pressure gradient. *Phys. Rev. Fluids* **2** (9), 092601.

Yang, Xiang I A, Hong, Jiarong, Lee, Myoungkyu & Huang, Xinyi L D 2021 Grid resolution requirement for resolving rare and high intensity wall-shear stress events in direct numerical simulations. *Phys. Rev. Fluids* **6**, 054603.

537 Yang, Xiang I A & Lv, Yu 2018 A semi-locally scaled eddy viscosity formulation for LES wall models
538 and flows at high speeds. *Theor Comp Fluid Dyn* **32**, 617–627.